Published in final edited form as:
Optom Vis Sci. 2014 August ; 91(8): 939–949. doi:10.1097/OPX.0000000000000323.

Cone Structure in Subjects with Known Genetic Relative Risk for AMD

Megan E. Land, BS, **Robert F. Cooper, BS**, **Jonathon Young**, **Elizabeth Berg, PhD**, **Terrie Kitchner**, **Qun Xiang, MS**, **Aniko Szabo, PhD**, **Lynn C. Ivacic**, **Kimberly E. Stepien, MD**, **C. David Page, PhD**, **Joseph Carroll, PhD**, **Thomas Connor Jr, MD**, and **Murray Brilliant, PhD**
Department of Ophthalmology (MEL, JY, KES, JC, TC, Jr.), Division of Biostatistics, Institute for Health and Society (QX, AS, CDP), Medical College of Wisconsin, Milwaukee, Wisconsin, Department of Biomedical Engineering, Marquette University, Marquette, Michigan (RFC), Department of Computer Sciences, University of Wisconsin-Madison, Madison, Wisconsin (EB), and Center for Human Genetics (TK, MB), Core Laboratory (LCI), Marshfield Clinic Research Foundation, Marshfield, Wisconsin (TK)

Abstract

Purpose—Utilize high resolution imaging to examine retinal anatomy in patients with known genetic relative risk (RR) for developing age-related macular degeneration (AMD).

Methods—Forty asymptomatic subjects were recruited (9 males, 31 females; 51–69 years, mean=61.4 years). Comprehensive eye exam, fundus photography and high-resolution retinal imaging using SD-OCT and adaptive optics (AO) were performed on each patient. Genetic RR scores were developed using an age-independent algorithm. AO scanning light ophthalmoscope (AOSLO) images were acquired in the macula extending to 10 degrees temporal and superior from fixation and were used to calculate cone density in up to 35 locations for each subject.

Results—RR was not significantly predictive of fundus grade ($p=0.98$). Only patients with a high RR displayed drusen on Cirrus or Bioptigen OCT. Compared to an eye with a grade of 0, an eye with a fundus grade ≥ 1 had a 12% decrease in density ($p<0.0001$) and a 5% increase in spacing ($p=0.0014$). No association between genetic RR and either cone density ($p=0.435$) or spacing ($p=0.538$) was found. Three distinct AOSLO phenotypical variations of photoreceptor appearance were noted in patients with grade 1–3 fundi. These included variable reflectivity of photoreceptors, decreased waveguiding, and altered photoreceptor mosaic overlying drusen.

Conclusions—Our data demonstrate the potential of multimodal assessment in the understanding of early anatomical changes associated with AMD. AOSLO imaging reveals a decrease in photoreceptor density and increased spacing in patients with grade 1–3 fundi, as well as a spectrum of photoreceptor changes, ranging from variability in reflectivity to decreased density. Future longitudinal studies are needed in genetically characterized subjects to assess the significance of these findings with respect to the development and progression of AMD.

Corresponding author: Murray Brilliant, 1000 N. Oak Ave, Marshfield, WI 54449, brilliant.murray@mcrf.mfldclin.edu.

Keywords

age-related macular denegeration; adaptive optics; photoreceptor

Age related macular degeneration (AMD) is a chronic, progressive disease resulting in the loss of central vision. AMD is characterized by the formation of extracellular deposits (drusen) between the retinal pigment epithelium (RPE) and Bruch's membrane. The presence of drusen is considered the earliest clinical sign of pathological changes associated with AMD.[1] As the disease progresses, the development of geographic atrophy (GA) of the RPE and choriocapillaris, as well as choroidal neovascularization can occur. AMD represents the leading cause of vision loss in the developed world,[2] and owing to the increasing life expectancy, morbidity related to AMD is projected to increase in prevalence in the coming decades.[3] Of those diagnosed with AMD, 85 – 90% of patients present with nonexudative, or, "dry" AMD.[4] Current clinical management of these patients involves supplementation with antioxidant vitamins and zinc,[5] as well as monitoring for metamorphopsia, which would suggest choroidal neovascularization and progression to "wet" AMD. However, many patients remain asymptomatic for quite some time, representing a window of opportunity to intervene before devastating vision loss occurs. Currently lacking, however, are objective structural biomarkers that can identify the earliest anatomical changes associated with AMD.

Recent advances in clinical imaging, such as spectral domain optical coherence tomography (SD-OCT), have greatly aided in the diagnosis and assessment of the progression of AMD, and have provided critical information for clinical decision-making. With its excellent axial resolution, SD-OCT has been used to characterize and classify different types of drusen.[6] However, the lateral resolution of commercial SD-OCT is insufficient to visualize structures at the cellular level, impeding the ability to characterize and recognize changes associated with the disease in its earliest stages. Adaptive optics (AO) imaging tools represent a potential solution to the inadequate resolution of traditional imaging modalities. While histologic studies have shown photoreceptor loss in both exudative and nonexudative AMD,[7] the use of AO imaging tools represents an opportunity for *in vivo* analysis of photoreceptor involvement in AMD. Recent studies using AO retinal imaging in the assessment of photoreceptor density in patients with AMD have shown differing results. Obata and Yanagi (2014) did not observe a difference in photoreceptor density between subjects with AREDS grade 1 fundi and those with an AREDS grade of 2 or 3.[8] However, a decrease in density corresponding to age and axial length was noted.[8] Boretsky *et al*. (2012) showed that patients exhibiting extensive drusen or GA display diminished cone density when compared to patients with small or intermediate drusen.[9] However, Zayit-Soudry *et al*. (2013) showed that patients with GA displayed continuous cone mosaics that were often of normal spacing, and that spacing was stable over time despite signs of clinical progression.[10] Godara *et al*. (2010) showed that photoreceptor density and mosaic were well-preserved overlying a basal laminar druse in an asymptomatic patient.[11] In addition, Querques *et al*. (2012) found an intact photoreceptor mosaic in a patient with large drusen, further supporting that photoreceptor loss may not occur until later in the disease process.[12] Mrejen *et al*. (2013) examined subjects with either conventional or pseudodrusen and found

a significant reduction in photoreceptor density overlying both conventional drusen (nearly 22%) and pseudodrusen (over 90%).[13] They also reported altered photoreceptor reflectivity overlying pseudodrusen. In most cases this was manifested as a ring of hyporeflectivity surrounding the deposit, however, photoreceptor structure was not discernible over many of the subretinal drusenoid deposits.[13]

We sought to identify the earliest anatomical changes associated with AMD by screening previously undiagnosed subjects (over the age of 50) selected primarily on the basis of having a high or low genetic relative risk (RR) for developing AMD. Examining these subjects provides an opportunity to further our understanding of the early stage of the disease process as well as to correlate changes seen with standard clinical imaging to those seen with AO imaging tools. This multimodal imaging approach may provide a more precise method for monitoring disease progression and identifying those at risk for development of the disease, ultimately allowing for intervention before vision loss.

MATERIALS AND METHODS

Genetic Relative Risk (RR) Algorithm

Genetic AMD RR scores were developed by comparing previously identified single nucleotide polymorphisms (SNPs) associated with AMD (http://www.genome.gove/gwastudies/) in 1,021 AMD cases (all ages) against 439 controls (individuals over age 70 with recent comprehensive eye exams that did not note AMD). The final algorithm was a logistic regression model that incorporated 5 of the 24 tested SNPs (rs10737680 and rs1329424 in *CFH*; rs3793917 in *ARMS/HTRA1*; rs641153 in *C2/CFB*; and rs493258 in *LIPC*). Under ten-fold cross-validation, a robust form of hold-out testing, this approach distinguishes cases from controls with an area under the receiver operating characteristic (ROC) curve, or an AUC, of 0.667. This algorithm is age-independent. Patients in the high-risk quartile had an RR above 1.4, while those in the low-risk quartile had an RR below 0.57 by age 70. Figure 1 displays the ROC curve and survival curves generated by the final genetic RR assessment algorithm.

Human Subjects

This study adhered to the tenets of the Declaration of Helsinki and was approved by the Medical College of Wisconsin and the Marshfield Clinic Research Foundation Institutional Review Boards. Participants provided written informed consent after explanation of the nature and possible consequences of the study. Thirty-five subjects included in the study were selected on the basis of having either a high or low genetic RR as determined above, while five asymptomatic adults with no diagnosis of AMD were prospectively recruited and had their genetic RR measured after imaging. Researchers involved in the imaging aspects of the study were masked to the genetic RR of the patients until all analyses were completed. Subjects were randomized to have either their right or left eye included in the study, with only one eye examined per subject. All subjects underwent a comprehensive ophthalmologic examination as well as fundus photography and imaging as described below. Color fundus photographs were evaluated and graded by a single ophthalmologist masked to the genetic RR assessment of the patients. A fundus grade of 0 was assigned if no drusen were present.

The remaining subjects were graded according to the severity scale for AMD as described in AREDS report number 17.[14] According to the AREDS nine-step severity scale described in this report, the presence of multiple abnormalities is assessed including largest drusen size, total drusen area, increased pigmentation, depigmentation, the presence of GA, and the presence of soft, indistinct drusen. Only one of the abnormalities needs to be present to achieve the given clinical grade, and the abnormality resulting in the highest possible grade is used for determining classification. In this report, inclusion criteria for a fundus grade of 1 include the questionable (≥50% likelihood but <90% likelihood) presence of a drusen, total drusen area between 63 and 125 μm, or the questionable presence of increased pigmentation, depigmentation, GA, or soft drusen. Inclusion criteria for a grade of 2 include largest drusen size <63 μm, total drusen area ≥125 μm but <250 μm, increased pigmentation area <63 μm, depigmentation area <354μm, or the presence of soft, indistinct drusen. Inclusion criteria for a grade of 3 include largest drusen size ≥63 μm but <125 μm, total drusen area ≥250 μm but <354 μm, increased pigmentation area ≥63 μm but <125 μm, depigmentation area ≥354 μm but <650 μm, or the presence of soft, indistinct drusen in one of three retinal zones.

Spectral-Domain Optical Coherence Tomography (SD-OCT)

Volumetric images of the macula were acquired using the Zeiss Cirrus HD-OCT (Carl Zeiss, Meditec, Dublin CA, USA). Volumes were nominally 6 mm×6 mm and consisted of 128 B-scans (512 A-scans/B-scan). The location of the foveal pit was determined using the FoveaFinder algorithm on the Cirrus software (v. 6.5.0772). RPE composite maps generated from Cirrus SD-OCT were evaluated for elevations, which would suggest the presence of drusen. Outer retinal layer integrity was assessed using high-resolution SD-OCT (Bioptigen, Inc., Durham, NC). Line scan sets were acquired (1000 A-scans/B-scan; 100 repeated B-scans) through the foveal center. Scans were registered and averaged as previously described to reduce speckle noise in the image.[15]

Microperimetry Testing

Microperimetry testing was obtained using an OPKO/OTI microperimeter (OPKO Instrumentation, Miami, FL). The protocol previously described by Anastasakis *et al*. (2011), was followed to obtain retinal sensitivity measurements.[16] This involved using the Polar 3 testing pattern, which includes 28 points arranged in 3 concentric circles (2.3, 6.6, and 11 degrees in diameter).[16] The stimulus was equal to the size of the Goldman III, with a 200-milisecond duration of presentation and 1.5 second interval between each stimulus presentation. Two trials were performed for each eye tested.

Adaptive Optics (AO) Retinal Imaging

Prior to imaging, the subject's eye was dilated and accommodation suspended using one drop each of phenylephrine hydrochloride (2.5%) and tropicamide (1%). An AO scanning light ophthalmoscope (AOSLO) was used to acquire images of the cone mosaic, and system details have been described in detail elsewhere.[17–19] The eye's monochromatic aberrations were compensated for using a deformable mirror (ALPAO S.A.S., Biviers, Grenoble, France). Image sequences (150 frames each) were acquired using a 796nm superluminescent diode (SLD) (Superlum, Carrigtwohill, Co. Cork, Ireland). Images were acquired at the

macula as well as extending approximately 10 degrees along the superior and temporal meridians.

Processing of AOSLO Image Sequences

In order to correct for distortions in the AOSLO images due to the sinusoidal motion of the resonant optical scanner, we first estimated the distortion from images of a Ronchi ruling, and then re-sampled the images over a grid of equally spaced pixels. After this "desinusoiding", the movies were manually inspected to identify reference frame(s) with minimal distortion and maximal sharpness for subsequent registration using custom software.[20] Registration of frames within a given image sequence was performed using a "strip" registration method, in which the images were registered by dividing the image of interest into strips, aligning each strip to the location in the reference frame that maximizes the normalized cross correlation between them.[20] Once all the frames were registered, the 50 frames with the highest normalized cross correlation to the reference frame were averaged, in order to generate a final image with an increased signal to noise ratio (SNR) for subsequent analysis. Final images were then manually stitched together using Adobe Photoshop (Adobe Systems, Inc., San Jose, CA) to generate a montage of the imaged area. AOSLO montages, Cirrus maps, fundus photographs, and Bioptigen scans were manually aligned using Adobe Photoshop (Adobe Systems Inc., San Jose, CA).

Analysis of Cone Density

Cone density was analyzed using the processed AOSLO images. To ensure the measurements across subjects were acquired relative to a common anatomical feature, we used the center of the foveal pit as determined by Cirrus OCT as the reference point for each subject. Cone density was measured over a 37 × 37 μm sampling window (to facilitate comparison with previous histological data[21]) at the foveal center and each of 34 additional regions of interest (0.25, 0.5, 0.75, 1.0, 1.5, 2.0, 2.5, 3.0, 3.5, 4.0, 4.5, 5.0, 6.0, 7.0, 8.0, 9.0, and 10.0 degrees relative to the location of foveal pit in both superior and temporal directions). Not all locations could be assessed for each subject due to poor image quality, the presence of vasculature, or incomplete montages. Images within 2 degrees of the fovea were counted using a semi-automated program.[22] Locations beyond 2 degrees were manually counted by a single observer (MEL) using ImageJ (Wayne Rasband, National Institutes of Health, Bethesda, MD; available at http://rsb.info.nih.gov/ij/index.html) due to the presence of rod photoreceptors confounding the automated algorithm. Figure 2 shows example images from regions of interest with cones marked for density and spacing measurements.

Statistical Analysis

Analyses were performed in SAS 9.3. (SAS institute, Cary, NC) using the MIXED procedure as the primary analyses. A general linear model analysis was used as this afforded the ability to adjust for the within-person correlation in the setting of repeated measurements as well as missing data (as a result of poor image quality, etc. as stated previously). For the correlation, a Kroenecker product structure with autoregressive correlation (AR(1)) between different angles along the same direction and unstructured correlation between the directions was used (selected using the Akaike Information Criterion). Cone density and spacing, log-

transformed for the analysis to stabilize the variance, were evaluated as a function of measurement position, fundus grade, and genetic RR. Interaction terms were used to evaluate whether the effect of measurement angle depended on the direction (temporal versus superior), and whether the effect of fundus grade and genetic RR depended on measurement location. The effects estimated on log-scale were back-transformed to and interpreted as fold-changes on the original scale.

RESULTS

Subject Characteristics

Subjects ranged in age from 51–69 years of age with a mean of 61.4 years. Thirty-one subjects were female, and nine were male. All patients had relatively preserved best-corrected visual acuity (BCVA) with a range of 20/13 to 20/32 (+1). Color vision defects identified included one male with protanopia, one male with deuteranomalous trichromacy, and one female who was an obligate carrier for an unknown form of color blindness. All others had normal color vision. Twenty-one subjects received a fundus grade of 0 (no drusen present), 14 received a fundus grade of 1 (total drusen area of 63–125 μm), four received a fundus grade of 2 (total drusen area of 125–250 μm with largest individual drusen size less than 63 μm), and one subject received a fundus grade of 3 (total drusen area of 250–354 μm with the largest individual drusen size 63–125 μm). Table 1 summarizes patient demographics.

Genetic Relative Risk (RR)

Twenty subjects were in the high RR quartile, sixteen were in the low RR quartile, and four were within the middle two risk quartiles. Of the 20 subjects in the high RR quartile; 11 had a fundus grade of 0, six had a fundus grade of 1, two had a fundus grade of 2, and one had a fundus grade of 3. Of the 16 subjects in the low-risk quartile, 10 had a fundus grade of 0, five had a fundus grade of 1, and one had a fundus grade of 2. Of the four subjects within the two middle risk quartiles, three had a fundus grade of 1, and one had a fundus grade of 2. High genetic RR for AMD was not predictive of an increased fundus grade ($p=0.98$).

SD-OCT Findings

Abnormalities observed on Bioptigen SD-OCT included disruption of the inner segment ellipsoid (ISe), disruption of the RPE, focal disruption of the outer segment and RPE layers at the fovea, attenuation of the external limiting membrane (ELM), and the presence of drusen. Twenty-one subjects had normal outer retinal structure on the Bioptigen SD-OCT. Of these, 12 were in the high RR quartile, and nine were in the low RR quartile. Three subjects had disruption of the ISe, with two of these subjects being in the high RR quartile, and one in the low RR quartile. Six subjects had focal disruption of the outer segment and RPE layers at the fovea, with two of these subjects being in the high RR quartile, and four in the low RR quartile. One subject showed attenuation of the ELM and was in the high RR quartile. One subject showed disruption of the ISe and RPE and was in the low RR quartile. Three subjects had drusen evident on both Cirrus and Bioptigen SD-OCT. All three of these subjects were in the high RR quartile. High genetic RR was not predictive of any abnormality on Bioptigen SD-OCT ($p=1$). However, only subjects with a high genetic RR

had drusen present on either Bioptigen or Cirrus SD-OCT. The small sample size of only three patients with evident drusen precluded any statistical significance of this finding.

Microperimetry

Subjects were determined to have decreased foveal sensitivity if they scored below 20 dB on both trials. In all other locations, a score below 10 dB on both trials was considered decreased sensitivity. Twenty-one patients had decreased foveal sensitivity. Of these, 11 were in the high RR category, nine were in the low RR category, and one was within the middle two quartiles. High genetic RR was not predictive of decreased foveal sensitivity ($p=0.95$). Twenty-six subjects had sensitivity below 10 dB on both trials in one or more of the other locations tested. Of these, 16 were in the high genetic RR category, and 10 were in the low genetic RR category. High genetic RR was not predictive of decreased sensitivity in these locations ($p=0.12$). Thirteen grade 0 subjects and 15 subjects with a fundus grade of 1 to 3 had decreased sensitivity at any location in both microperimetry trials. Fundus grade was not predictive of decreased microperimetry sensitivity ($p=0.71$). Thirteen grade 0 subjects and 11 subjects with a fundus grade of 1 to 3 had decreased foveal sensitivity. Increased fundus grade was not found to be associated with decreased foveal sensitivity ($p=0.97$).

Adaptive Optics Photoreceptor Density

AO images for all subjects that had been assigned a fundus grade of 0 were examined. Of these, only eight subjects displayed highly discernible cone morphology and were subsequently used for analysis purposes. These eight subjects that had been assigned a fundus grade of 0 were compared to previously published data obtained through either histology or AO imaging.[21,23] As shown in Figure 3, density measurements obtained in these subjects corresponded closely with this previously published data. However, unlike Song *et al.* (2001), our data did not show an age-related decrease in photoreceptor density.[23] Data were also compared to a cohort of individuals (7 males, 2 females; mean age = 25 years) without ocular pathology that had previously been imaged using the same AOSLO system. A general linear model analysis was utilized to examine cone density and there was no significant difference in density between this group and the grade 0 subjects ($p=0.165$). We next compared our grade 0 subjects to subjects with a grade 1 or 2 fundus to evaluate differences in photoreceptor density as a function of fundus grade and genetic RR. As with the grade 0 subjects, only subjects with highly discernible cone morphology were subsequently used for analysis purposes (grade 1, n=11; grade 2, n=3). Figure 4 shows example images from various regions of interest used for cone density and spacing measurements.

Photoreceptor Density and Spacing as a Function of Grade and Genetic RR

A general linear model analysis was used to examine the association of fundus grade with respect to cone density and spacing, controlling for photoreceptor density and spacing as repeated measurements. Grade 1 and 2 subjects were combined due to the small number of grade 2 subjects in this study population. The results show that subjects with a fundus grade of 1 or 2 had a significant reduction in cone density and a significant increase in cone

spacing. Compared to the 8 eyes with a grade 0 fundus for whom we analyzed cone density, eyes with a fundus grade of 1 or more (n=14) had a 12% decrease in density ($p<0.0001$) and a 5% increase in spacing ($p=0.0014$). These changes are assumed to be uniform across all locations measured as the addition of an interaction term was not significant, in other words, there was not enough evidence to suggest a non-uniform reduction in cone density across the retinal locations assessed. A similar analysis was conducted using RR as a predictor of cone density and spacing, however, no association between genetic RR and either cone density ($p=0.435$) or spacing ($p=0.538$) was found.

AOSLO Qualitative Abnormalities

Three distinct patterns of qualitative photoreceptor abnormalities were noted on AOSLO. These included abnormal reflectivity of photoreceptors, annular rings of hyporeflectivity surrounding drusen with an intact overlying photoreceptor mosaic, and those with a disrupted photoreceptor mosaic overlying drusen.

As shown in Figure 5, two grade 1 patients and one grade 2 patient showed a complete and contiguous photoreceptor mosaic, however, there were several patches of photoreceptors showing lower frequency changes in reflectivity. No overt abnormalities were noted in these patients on SD-OCT other than subtle changes at the level of the RPE. Figure 6 displays the second phenotype in which four grade 1 patients displayed annular rings of hyporeflectivity on the edges of drusen. In this phenotype, the photoreceptor mosaic remained intact, but displacement of the photoreceptor layer induced by space-occupying drusen disrupts the waveguiding of the photoreceptors found on the edge of the drusen. The photoreceptors near the edge of drusen were more easily visualized when displayed on a logarithmic scale. Despite these alterations in waveguiding, a complete contiguous photoreceptor mosaic remained, similar to previously published observations.[11]

Two grade 2 subjects and the grade 3 subject showed drusen with an overlying disruption of the photoreceptor mosaic. Individual photoreceptors could not be visualized in these areas, even when viewed on a logarithmic scale. This is represented in Figure 6. However, when viewed on SD-OCT, these patients displayed an intact-appearing ISe band.

DISCUSSION

Our data demonstrate the potential of multimodal assessment for understanding early anatomical changes associated with AMD. The combination of AOSLO, standard clinical imaging, and genetic risk stratification provides a valuable approach to study this disease. Many of the abnormalities noted on AOSLO were not visible with standard clinical imaging, highlighting the sensitivity of AO imaging for studying the earliest anatomical changes associated with AMD.

Genetic RR was not predictive of increased AREDS fundus grade. However, consistent with the AREDS grading system, drusen anywhere within the arcades were considered for grading purposes. Many of these drusen were not within the area visualized with OCT, and are thus unlikely to interfere with daily visual functioning. Although it did not reach significance, only patients with a high genetic RR displayed drusen visible on OCT, whereas

none of the patients with low genetic RR had drusen seen on OCT. This suggests that genetic RR may be useful in predicting the evolution of clinically disruptive drusen. Future longitudinal studies with larger sample sizes of genetically characterized subjects will be needed to further investigate this hypothesis.

Decreased foveal sensitivity on microperimetry was not found to be associated with high genetic RR or increased fundus grade. Decreased sensitivity at any of the locations tested was also not found to be associated with high genetic RR or increased fundus grade. Previous studies utilizing microperimetry testing in subjects already with a diagnosis of AMD (based on fundus appearance) have found a significant reduction in retinal sensitivity overlying drusen as well as at the margins of GA.[24] A significant correlation between retinal sensitivity and drusen volume as well as absolute scotomas overlying areas of GA was also noted.[24] This suggests that a decrease in retinal sensitivity as measured by microperimetry testing is likely a later change that worsens as the disease progresses.

Photoreceptor density measurements in our subjects corresponded closely with previously published data.[21, 23] However, our data did not demonstrate a decrease in photoreceptor density related to age, as previously described.[8,23] This may be because the subjects included in this cohort in our study all had grade 0 fundi. Perhaps earlier studies not accounting for fundus grade may have incorporated subjects with pre-clinical AMD, resulting in decreased density measurements. Using flood-illuminated AO imaging, Obata and Yanagi (2014) did not find a decrease in photoreceptor density in subjects with grade 2 or 3 fundi compared with grade 1 subjects.[8] This is in contrast to our study's findings, however Obata and Yanagi (2014) only compared subjects with different grades of AMD whereas ours included subjects with any classification of AMD and compared those to age matched normals. This results in our study having an increased sensitivity to detect for the earliest AMD-associated changes in photoreceptor density. In contrast to Zayit-Soudry *et al*. (2013), our study found that subjects with a fundus grade of 1 or more showed a decrease in cone density and an increase in cone spacing compared with eyes with a grade 0 fundus.[10] Zayit-Soudry *et al*. (2013) evaluated eight eyes of seven patients with either intermediate AMD or GA. They found that in the majority of cases, subjects had normal cone spacing both in areas overlying drusen and on the border of GA and that this spacing remained normal during the study's follow up period (12 to 21 months).[10] However, our findings of decreased photoreceptor density in patients with increased fundus grade is similar to Mrejen *et al*. (2013), who observed a significant reduction in photoreceptor density overlying both drusen and pseudodrusen.[13]

Similar to findings in patients with AMD,[10,13] qualitative photoreceptor abnormalities were noted in our patients, including abnormal reflectivity of photoreceptors, annular rings of hyporeflectivity surrounding drusen, and a disrupted photoreceptor mosaic overlying drusen. The fact that some of the same photoreceptor changes were found in patients diagnosed with bona fide AMD suggests that the changes seen in our patients are indeed linked to the disease process. Previous studies have shown that changes at the level of the RPE can result in alterations in photoreceptor reflectance on AO images.[25] Although the exact mechanism of drusen formation remains unclear, one hypothesis is that RPE cell degeneration may create cellular debris that serves as the impetus of a chronic inflammatory state and that this

chronic inflammatory state may initiate drusen formation.[26] Thus, the subtle changes in photoreceptor reflectivity may be one of the earliest anatomical changes associated with AMD and could be indicative of RPE cell dysfunction. In this case, the three described phenotypes would represent a continuum of disease states beginning with an altered RPE, progressing to the formation of drusen, and ultimately to the deterioration of photoreceptors; as the loss of photoreceptors is known to be associated with AMD as previously described in histology[7] and more recently by AO.[9]

Several challenges exist in the imaging of the aged eye. These patients are prone to several age-related changes including smaller pupil size, media opacities, cataract formation, and abnormalities in the tear film; all of which reduce the quality of images acquired using AOSLO. The variation in image quality attained from various subjects represents a possible limitation of studies like ours. Many areas had unacceptable image quality necessary for the evaluation of photoreceptor density and spacing, and were subsequently omitted from analysis. This could result in a more conservative estimate of the changes in photoreceptor density and spacing as they relate to the earliest signs of AMD. More advances are needed in AO technology, specifically with regard to improvements designed for imaging the aged eye. In addition, it is often difficult to distinguish normal age-related changes from those that indicate a disease state. For example, the presence of fine, hard drusen can be considered a normal response to aging,[27] however, they are also one of the criteria considered for AMD grading using the AREDS severity scale for age-related macular degeneration.[14] Thus, future longitudinal studies will be needed in order to disambiguate normal age-related anatomical changes from those specific to AMD progression. Although limitations exist, the potential of AOSLO imaging to assist in better understanding, diagnosis, and ultimately treatment of diseases such as AMD is great.

Acknowledgments

This study was funded by grants from the Wisconsin Genome Initiative, Research to Prevent Blindness, the Gene and Ruth Posner Foundation, and the RD & Linda Peters Foundation. This study was partially supported by NIH grants U01HG006389, and P30EY001931. This investigation was conducted in part in a facility constructed with support from the Research Facilities Improvement Program; Grant C06RR016511 from the National Center for Research Resources, National Institutes of Health. This project was supported in part by the National Center for Advancing Translational Sciences, National Institutes of Health, through grant numbers UL1TR000055 and UL1TR000427. Its contents are solely the responsibility of the authors and do not necessarily represent the official views of the NIH.

REFERENCES

1. Pauleikhoff D, Barondes MJ, Minassian D, Chisholm IH, Bird AC. Drusen as risk factors in age-related macular disease. Am J Ophthalmol. 1990; 109:38–43. [PubMed: 1688685]
2. Rein DB, Zhang P, Wirth KE, Lee PP, Hoerger TJ, McCall N, Klein R, Tielsch JM, Vijan S, Saaddine J. The economic burden of major adult visual disorders in the United States. Arch Ophthalmol. 2006; 124:1754–1760. [PubMed: 17159036]
3. Rein DB, Wittenborn JS, Zhang X, Honeycutt AA, Lesesne SB, Saaddine J. Forecasting age-related macular degeneration through the year 2050: the potential impact of new treatments. Arch Ophthalmol. 2009; 127:533–540. [PubMed: 19365036]
4. Klein R, Chou CF, Klein BE, Zhang X, Meuer SM, Saaddine JB. Prevalence of age-related macular degeneration in the US population. Arch Ophthalmol. 2011; 129:75–80. [PubMed: 21220632]

5. Chew EY, Clemons TE, Agron E, Sperduto RD, Sangiovanni JP, Kurinij N, Davis MD. Long-term effects of vitamins C and E, beta-carotene, and zinc on age-related macular degeneration: AREDS report no. 35. Ophthalmology. 2013; 120:1604–1611. e4. [PubMed: 23582353]
6. Khanifar AA, Koreishi AF, Izatt JA, Toth CA. Drusen ultrastructure imaging with spectral domain optical coherence tomography in age-related macular degeneration. Ophthalmology. 2008; 115:1883–1890. [PubMed: 18722666]
7. Curcio CA, Medeiros NE, Millican CL. Photoreceptor loss in age-related macular degeneration. Invest Ophthalmol Vis Sci. 1996; 37:1236–1249. [PubMed: 8641827]
8. Obata R, Yanagi Y. Quantitative analysis of cone photoreceptor distribution and its relationship with axial length, age, and early age-related macular degeneration. PLoS One. 2014; 9:e91873. [PubMed: 24632778]
9. Boretsky A, Khan F, Burnett G, Hammer DX, Ferguson RD, van Kuijk F, Motamedi M. In vivo imaging of photoreceptor disruption associated with age-related macular degeneration: A pilot study. Lasers Surg Med. 2012; 44:603–610. [PubMed: 22930575]
10. Zayit-Soudry S, Duncan JL, Syed R, Menghini M, Roorda AJ. Cone structure imaged with adaptive optics scanning laser ophthalmoscopy in eyes with nonneovascular age-related macular degeneration. Invest Ophthalmol Vis Sci. 2013; 54:7498–7509. [PubMed: 24135755]
11. Godara P, Siebe C, Rha J, Michaelides M, Carroll J. Assessing the photoreceptor mosaic over drusen using adaptive optics and SD-OCT. Ophthalmic Surg Lasers Imaging. 2010; 41:S104–S108.
12. Querques G, Massamba N, Guigui B, Lea Q, Lamory B, Soubrane G, Souied EH. In vivo evaluation of photoreceptor mosaic in early onset large colloid drusen using adaptive optics. Acta Ophthalmol. 2012; 90:e327–e328. [PubMed: 21883987]
13. Mrejen S, Sato T, Curcio CA, Spaide RF. Assessing the cone photoreceptor mosaic in eyes with pseudodrusen and soft Drusen in vivo using adaptive optics imaging. Ophthalmology. 2014; 121:545–551. [PubMed: 24183341]
14. Davis MD, Gangnon RE, Lee LY, Hubbard LD, Klein BE, Klein R, Ferris FL, Bressler SB, Milton RC. The Age-Related Eye Disease Study severity scale for age-related macular degeneration: AREDS Report No. 17. Arch Ophthalmol. 2005; 123:1484–1498. [PubMed: 16286610]
15. Tanna H, Dubis AM, Ayub N, Tait DM, Rha J, Stepien KE, Carroll J. Retinal imaging using commercial broadband optical coherence tomography. Br J Ophthalmol. 2010; 94:372–376. [PubMed: 19770161]
16. Anastasakis A, McAnany JJ, Fishman GA, Seiple WH. Clinical value, normative retinal sensitivity values, and intrasession repeatability using a combined spectral domain optical coherence tomography/scanning laser ophthalmoscope microperimeter. Eye (Lond). 2011; 25:245–251. [PubMed: 21178993]
17. Sulai YN, Dubra A. Adaptive optics scanning ophthalmoscopy with annular pupils. Biomed Opt Express. 2012; 3:1647–1661. [PubMed: 22808435]
18. Cooper RF, Dubis AM, Pavaskar A, Rha J, Dubra A, Carroll J. Spatial and temporal variation of rod photoreceptor reflectance in the human retina. Biomed Opt Express. 2011; 2:2577–2589. [PubMed: 21991550]
19. Dubra A, Sulai Y. Reflective afocal broadband adaptive optics scanning ophthalmoscope. Biomed Opt Express. 2011; 2:1757–1768. [PubMed: 21698035]
20. Dubra, A.; Harvey, Z. Registration of 2D images from fast scanning ophthalmic instruments. In: Fischer, B.; Dawant, B.; Lorenz, C., editors. Biomedical Image Registration. Berlin: Springer-Verlag Berlin Heidelberg; 2010. p. 60-71.
21. Curcio CA, Sloan KR, Kalina RE, Hendrickson AE. Human photoreceptor topography. J Comp Neurol. 1990; 292:497–523. [PubMed: 2324310]
22. Garrioch R, Langlo C, Dubis AM, Cooper RF, Dubra A, Carroll J. Repeatability of in vivo parafoveal cone density and spacing measurements. Optom Vis Sci. 2012; 89:632–643. [PubMed: 22504330]
23. Song H, Chui TY, Zhong Z, Elsner AE, Burns SA. Variation of cone photoreceptor packing density with retinal eccentricity and age. Invest Ophthalmol Vis Sci. 2011; 52:7376–7384. [PubMed: 21724911]

24. Hartmann KI, Bartsch DU, Cheng L, Kim JS, Gomez ML, Klein H, Freeman WR. Scanning laser ophthalmoscope imaging stabilized microperimetry in dry age-related macular degeneration. Retina. 2011; 31:1323–1331. [PubMed: 21540764]

25. McAllister JT, Dubis AM, Tait DM, Ostler S, Rha J, Stepien KE, Summers CG, Carroll J. Arrested development: high-resolution imaging of foveal morphology in albinism. Vision Res. 2010; 50:810–817. [PubMed: 20149815]

26. Anderson DH, Mullins RF, Hageman GS, Johnson LV. A role for local inflammation in the formation of drusen in the aging eye. Am J Ophthalmol. 2002; 134:411–431. [PubMed: 12208254]

27. Ardeljan D, Chan CC. Aging is not a disease: distinguishing age-related macular degeneration from aging. Prog Retin Eye Res. 2013; 37:68–89. [PubMed: 23933169]

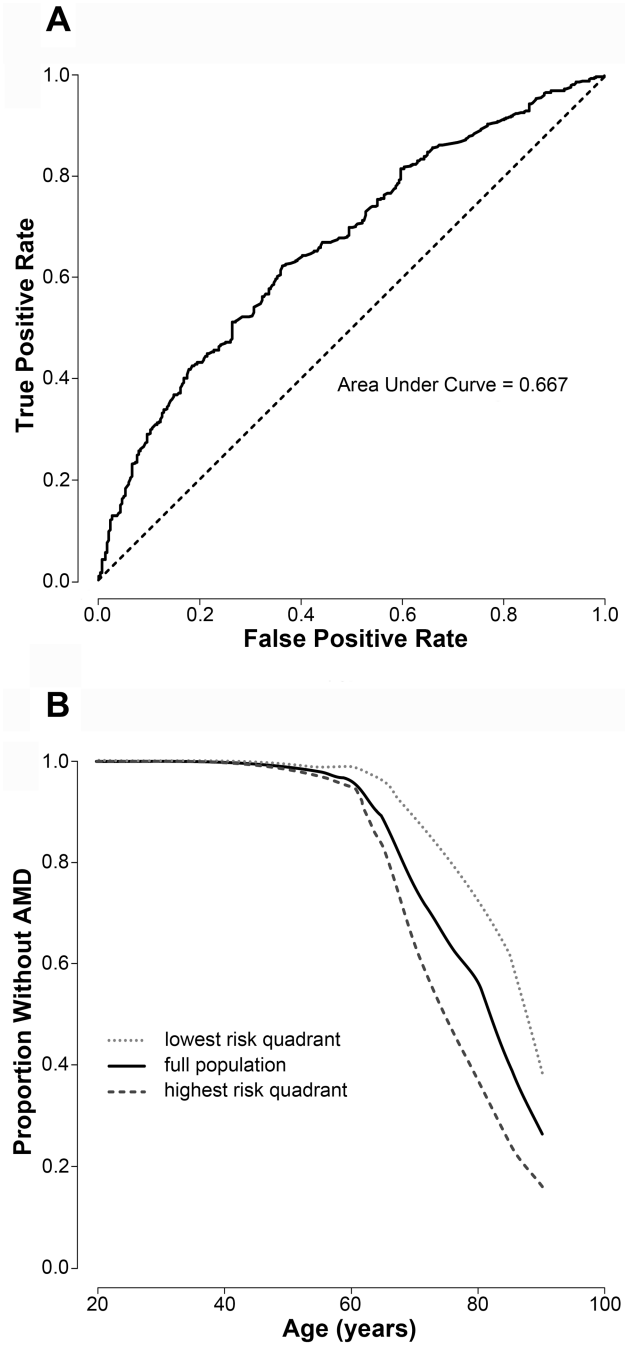

Figure 1.

Genetic Risk Algorithm. **(A)** Receiver Operating Characteristic Curve illustrating the performance of the binary classification of genetic relative risk for age related macular degeneration at various discrimination thresholds. **(B)** Survival curve demonstrating distribution of patients without AMD classified as either low or high genetic relative risk as a function of age.

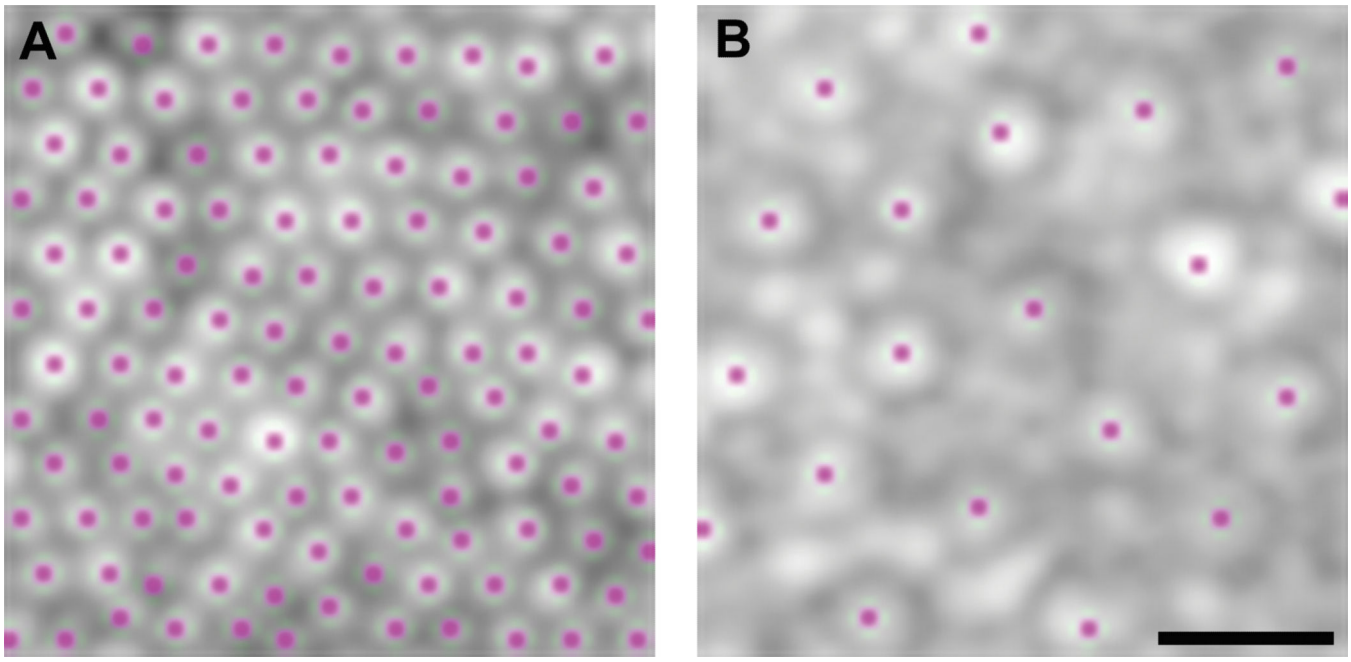

Figure 2.

Photoreceptor Selection for Density Measurement. Example of selection of cone photoreceptors at various locations for density and spacing measurements. **(A)** 0.25 Degrees Superior from Fovea. **(B)** 5.0 Degrees Temporal from Fovea. The presence of rod photoreceptors in peripheral locations necessitates manual cone photoreceptor detection. Scale bar is 10μm.

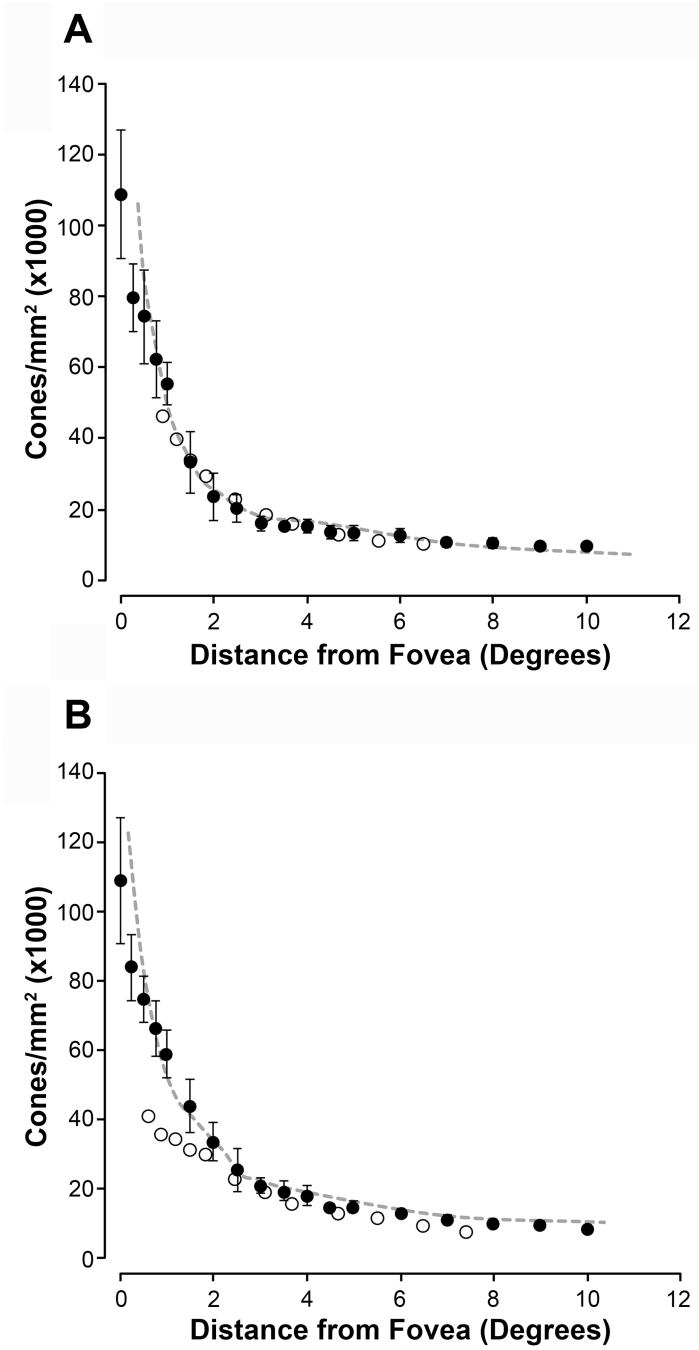

Figure 3.

Cone Density in Control Subjects vs. Previously Published Data. Shown are cone photoreceptor density measurements (filled circles) along the superior and temporal meridians in the grade 0 subjects along the superior **(A)** and temporal **(B)** meridia. Error bars represent ±1 standard deviation. Dashed gray line and open circles represent previously published normative data from Curcio et al. (1990) and Song et al. (2011), respectively.[21,23] The cone density from our grade 0 subjects corresponds closely with these previously published data sets.

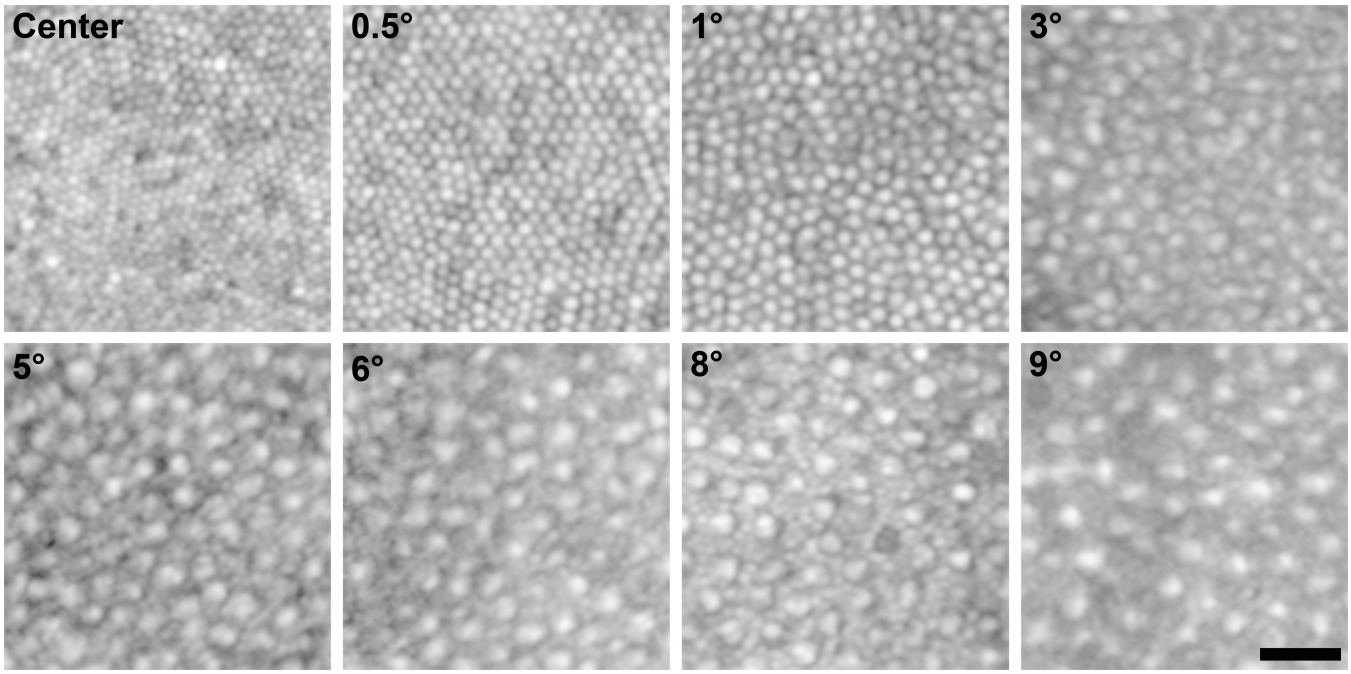

Figure 4.

Example Regions of Interest. Shown are AOLSO images of the cone mosaic from various regions of interest along the temporal meridian in a single subject. Images are shown in logarithmic display to minimize differences in individual photoreceptor brightness, making visualization of cells in the mosaic easier. Labels in each panel represent the retinal eccentricity of that image. Scale bar is 20μm.

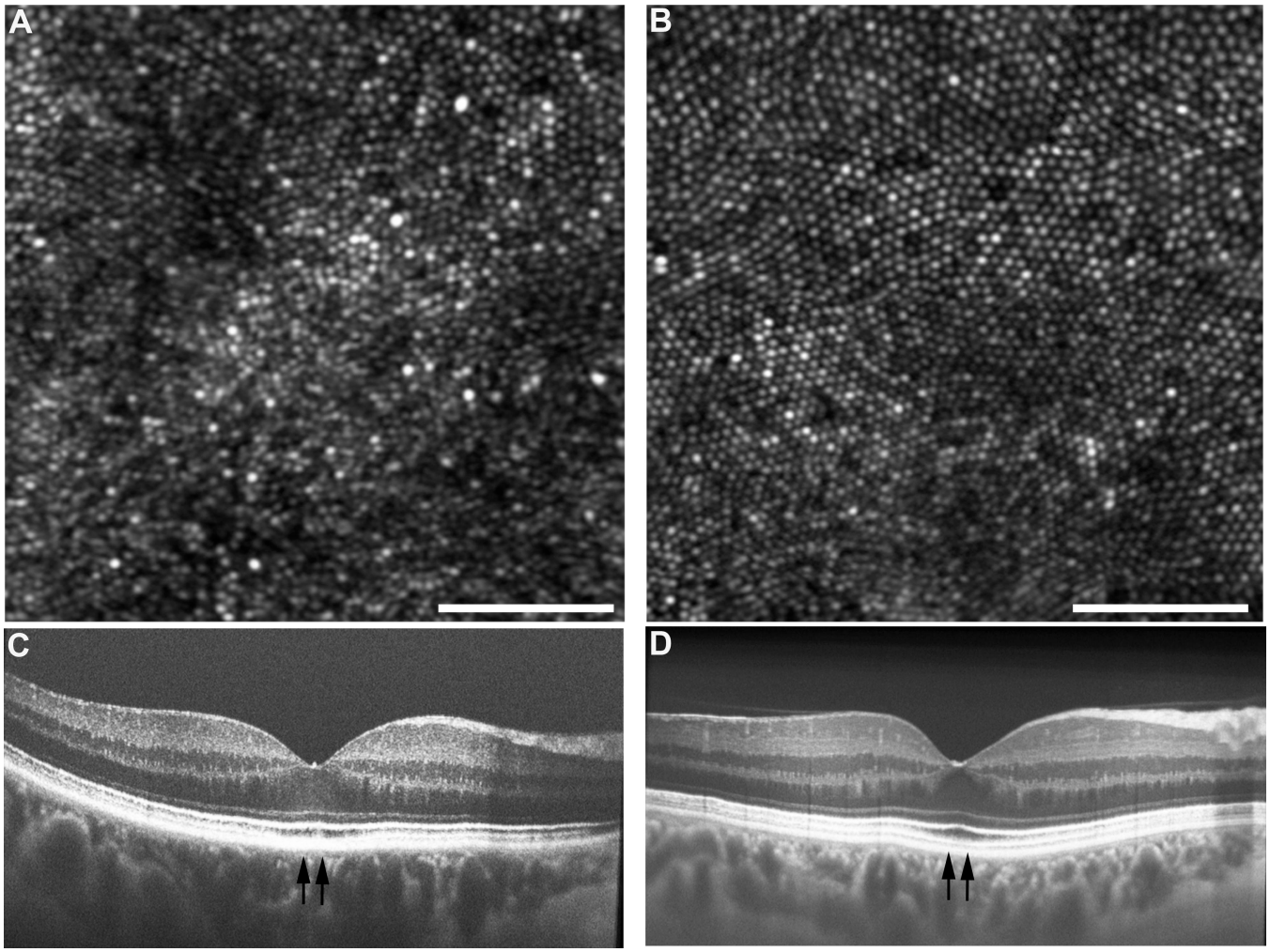

Figure 5.

Phenotype 1: Abnormal Reflectivity. In three subjects, no discrete drusen were present, however, individual photoreceptors had more highly variable reflectivity in the AOSLO images. **(A)** In JC_0926, lower-frequency changes in reflectance were observed and are consistent with changes at the level of the RPE. **(B)** Shown for comparison is JC_0823, an age-matched normal with a more uniform mosaic. Scale bar = 50μm. Corresponding SD-OCT from the subject with abnormal reflectivity **(C)** and from the subject with a normal-appearing mosaic **(D)**. Vertical arrows indicate the region imaged with AOSLO shown in panels A and B, respectively.

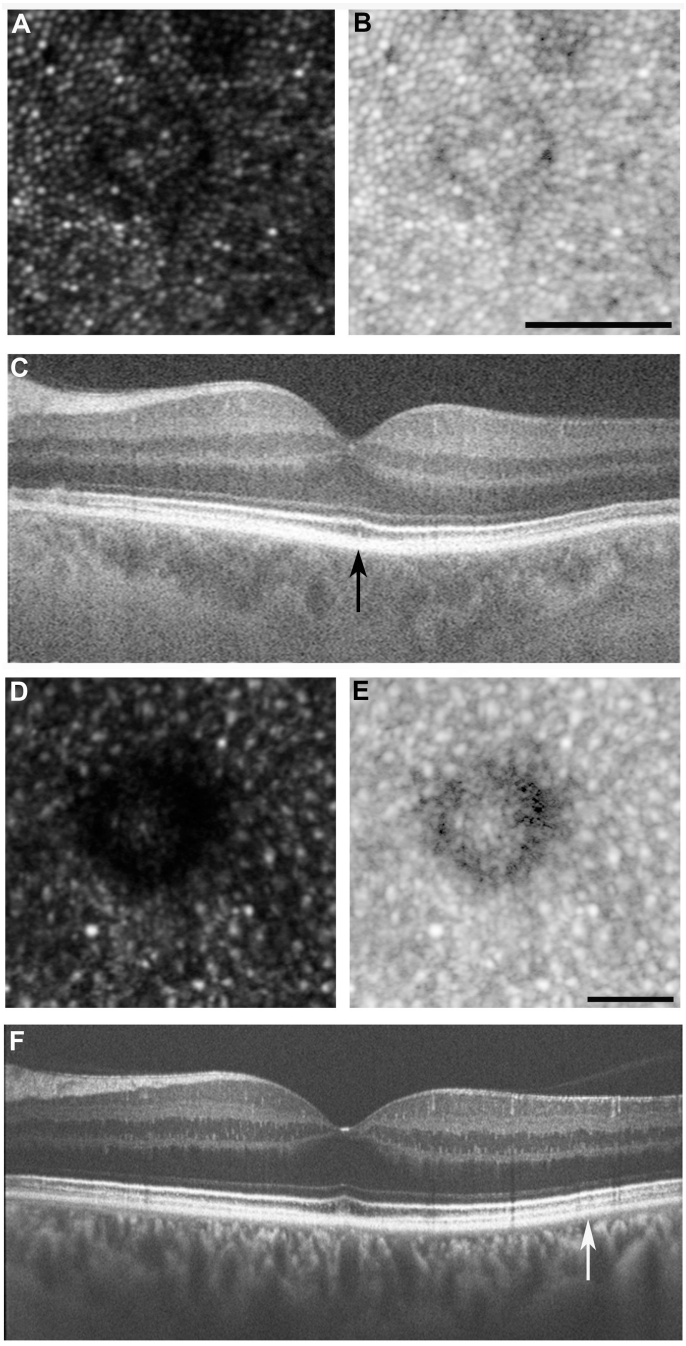

Figure 6.

Phenotypes 2 and 3: Decreased waveguiding and disrupted photoreceptor mosaic. Drusen were present in four subjects in which the overlying photoreceptor mosaic was undisturbed, consistent with previous observations.[11] Interestingly, the photoreceptors on the edge of these drusen had diminished reflectivity. This is most likely due to the Stiles-Crawford effect; where the three dimensional druse alters the trajectory of the reflected light. **(A)** AOSLO image from subject JC_0803, displaying decreased waveguiding phenotype. **(B)** Logarithmic view of AOSLO image. Scale bar = 50 μm. **(C)** Corresponding OCT, with

region imaged with AOSLO marked with vertical black arrow. In three subjects, drusen were present and the overlying photoreceptor mosaic was disturbed. By viewing on a logarithmic scale, it is evident that the photoreceptors are no longer discernable on the edge of drusen. These photoreceptor changes were not detected on SD-OCT. **(D)** AOSLO image from subject JC_1018, displaying disrupted photoreceptor mosaic. **(E)** Logarithmic view of AOSLO image. Scale bar = 50μm. **(F)** Corresponding SD-OCT, with region imaged with AOSLO marked with vertical white arrow.

Optom Vis Sci. Author manuscript; available in PMC 2015 August 01.

Table 1

Patient demographics.

Subject ID	Age	Sex	Eye	Axial Length (mm)	BCVA	Grade	RR Category	Color Vision
JC_0629	69	F	OS	22.6	20/25(+2)	2	Medium	Normal
JC_0648	61	F	OS	22.77	20/16(−1)	1	Low	Normal
JC_0649	65	F	OD	24.47	20/20(+3)	1	Medium	Normal
JC_0650	65	F	OD	24.81	20/20	1	Medium	Normal
JC_0797	61	F	OS	25.55	20/32(+3)	0	High	Normal
JC_0802	62	M	OD	22.27	20/25	0	Low	Protanope
JC_0803	62	M	OS	24.57	20/16	1	High	Normal
JC_0813	66	F	OD	22.99	20/20	0	Low	Normal
JC_0814	58	M	OS	23.82	20/25(+3)	0	Low	Normal
JC_0822	66	M	OD	24.94	20/16(−1)	0	Low	Deuteranomalous
JC_0823	52	F	OD	22.32	20/16(−1)	0	Low	Normal
JC_0825	63	F	OS	26.34	20/20	0	Low	Normal
JC_0854	61	F	OD	25.01	20/20	0	High	Normal
JC_0855	56	F	OS	23.39	20/20(+3)	0	High	Normal
JC_0856	59	F	OD	21.76	20/16(−1)	1	Low	Normal
JC_0864	56	M	OD	24.01	20/16(+2)	0	Low	Normal
JC_0865	62	F	OS	24.51	20/25(+3)	1	High	Normal
JC_0866	51	F	OD	25.61	20/20(+1)	1	High	Normal
JC_0877	60	F	OS	24.87	20/32(+1)	0	Low	Normal
JC_0883	64	M	OS	25.77	20/16(+3)	2	High	Normal
JC_0884	66	F	OD	24.11	20/32(+2)	1	Low	Normal
JC_0886	67	F	OS	25.08	20/32(+3)	0	High	Normal
JC_0908	57	M	OS	23.66	20/13	2	High	Normal
JC_0925	63	F	OD	22.76	20/25(+3)	0	Low	Normal*
JC_0926	66	F	OD	22.99	20/16	1	High	Normal
JC_0948	59	F	OS	25.56	20/16	0	High	Normal

Subject ID	Age	Sex	Eye	Axial Length (mm)	BCVA	Grade	RR Category	Color Vision
JC_1008	64	M	OS	25.03	20/20	3	High	Normal
JC_1009	59	F	OS	26.67	20/16(−1)	0	High	Normal
JC_1010	58	M	OS	23.66	20/16(+1)	0	High	Normal
JC_1018	58	F	OS	23.29	20/16(−1)	1	Medium	Normal
JC_1019	62	F	OD	24.96	20/25(+2)	1	Low	Normal
JC_1030	65	F	OS	24.97	20/20(+2)	0	High	Normal
JC_1032	64	F	OD	22.97	20/20	0	High	Normal
JC_1049	53	F	OD	24.9	20/13	1	High	Normal
JC_1061	65	F	OS	23.27	20/16(−1)	1	Low	Normal
JC_1062	58	F	OS	23.5	20/20	2	Low	Normal
JC_1066	65	F	OS	23.59	20/16(+1)	1	High	Normal
JC_1067	64	F	OS	23.26	20/20(+3)	0	High	Normal
JC_1069	56	F	OD	24.84	20/13(−1)	0	Low	Normal
JC_1075	66	F	OS	27.02	20/32(+3)	0	High	Normal

* Carrier for unknown form of colorblindness.

OS=left eye, OD=right eye, ND=not done, BCVA=best corrected visual acuity, RR=relative risk